

Article

Experiments and Simulations to Describe Alkalinity Release from Particle-Containing Oil-in-Water Emulsions and Particle Suspensions

Katherine A. Muller [†] and C. Andrew Ramsburg ^{*}

Department of Civil & Environmental Engineering, Tufts University, Medford, MA 02155, USA

^{*} Correspondence: andrew.ramsburg@tufts.edu; Tel.: +1-617-627-3211[†] Current Affiliation Pacific Northwest National Laboratory, Richland, WA 99352, USA.

Abstract: Among the most common amendments added to groundwater during site remediation are compounds used to adjust or maintain the pH. This research describes an approach to encapsulate mineral particles (MgO and $CaCO_3$) within oil droplets suspended within an aqueous phase for the purpose of delivery to the subsurface environment. A series of batch experiments was combined with mathematical modeling to illustrate the encapsulation and understand the influence of particle encapsulation on rates and extents of alkalinity release. The encapsulation of the alkalinity-releasing particles results in slower rates of amendment release as compared to rates obtained using suspensions of bare mineral particles, allowing for the possibility of control as a function of the pH. The results indicate that the alkalinity release from particle suspensions followed a mineral dissolution mechanism that could not explain the rate of the alkalinity release of the encapsulated particles. The reduction in mineral dissolution rates observed with the encapsulated particles was found to result from a mass transfer limitation. This limitation was well described using a linear driving force expression to account for the resistance to mass transfer at the oil–water interface.

Keywords: pH adjustment; buffer; alkalinity; EVO; stabilization; controlled release; groundwater; remediation



Citation: Muller, K.A.; Ramsburg, C.A. Experiments and Simulations to Describe Alkalinity Release from Particle-Containing Oil-in-Water Emulsions and Particle Suspensions. *Water* **2023**, *15*, 1611. <https://doi.org/10.3390/w15081611>

Academic Editor: Aldo Fiori

Received: 2 March 2023

Revised: 8 April 2023

Accepted: 18 April 2023

Published: 20 April 2023



Copyright: © 2023 by the authors. Licensee MDPI, Basel, Switzerland. This article is an open access article distributed under the terms and conditions of the Creative Commons Attribution (CC BY) license (<https://creativecommons.org/licenses/by/4.0/>).

1. Introduction

Many in situ remediation technologies hinge on the ability to adjust or control subsurface pH levels (e.g., bioremediation, metal stabilization and immobilization and chemical oxidation). In the case of the bioremediation of chlorinated solvents, for example, a high or low pH can diminish microbial activity and result in the accumulation of toxic compounds associated with a partial transformation, e.g., [1,2]. Thus, maintaining the pH at a near neutral level is critical for contaminant degradation to proceed [3]. Since reductive dechlorination itself generates acidic byproducts, the natural buffering capacity of the system is often overcome as the remediation progresses. Once the natural buffering capacity of the soil and waters is exhausted, an additional source of alkalinity is required to maintain the pH, e.g., [4–6].

While there are many approaches to deliver and distribute amendments in the subsurface, most artificial pH modification methods rely on aqueous-phase injections of alkaline solutions (e.g., carbonates and bicarbonates), soluble buffered solutions (e.g., phosphate buffers) or solid-phase alkaline minerals dissolved into a solution before use (e.g., $Mg(OH)_2$, CaO and $CaCO_3$), e.g., [3,7,8]. In practice, the transport and distribution of aqueous amendments is dependent on the ambient groundwater flow, which creates limitations related to an effective distribution throughout the aquifer. Additionally, aqueous injections frequently result in a temporary treatment, as soluble amendments move through the target zone with groundwater flow. As a result, engineers rely on multiple or continuous injections, or more aggressive control of the site hydrodynamics.

Alternatives to the delivery of dissolved phase amendments include the use of particle suspensions, the encapsulation of buffering agents and particles and mobility control agents. Insoluble colloidal suspensions of calcium carbonate particles [9] and silicate minerals [2] have been used to support pH control during remediation. However, particle suspensions are also prone to subsurface delivery challenges and provide little in the way of specific pH control as the rate and extent of alkalinity release is governed by mineral dissolution. Some studies suggest the use of mobility agents in the form of viscous fluids to potentially increase particle migration when establishing a treatment zone in the subsurface [10,11]. The use of viscous agents can be limited by the establishment of hydraulic gradients necessary to generate the flow of the mobility agent, especially in relatively shallow unconfined groundwater systems, e.g., [12,13]. Release kinetics have been modified by encapsulating active ingredients in macrocapsules, but millimeter-scale capsules restrict their application to systems amenable to physical mixing [14–16].

Mixtures of emulsified vegetable oil (EVO) for electron donor, colloidal Mg(OH)₂ for the buffer capacity and a reductive dechlorinating inoculum were shown to support the degradation of a dense nonaqueous-phase liquid (DNAPL) comprising tetrachloroethene [7]. At the field scale, a mixture of colloidal Mg(OH)₂ and EVO was injected through the aquifer to form permeable reactive barriers at a DNAPL site to enhance the reductive dechlorination and provide pH control [17]. The Mg(OH)₂ suspension itself was found to preferentially transport through the more permeable zones of the aquifer. Some of the Mg(OH)₂ suspension also settled in the injection wells, creating zones of prolonged high pH levels nearby.

The encapsulation of the alkalinity-releasing particles within the emulsified vegetable oil may reduce the previously observed settling or preferential transport of alkalinity-releasing particles. In addition, we hypothesize that encapsulating alkalinity-releasing particles within oil droplets of an oil-in-water emulsion may provide kinetic control on rates of alkalinity release that could serve to increase the duration of a treatment. Emulsions are extensively used in the pharmaceutical and food industries to encapsulate, deliver and release active constituents. Within the environmental sector, emulsions have been developed for many applications, including the delivery of fermentable substrates in enhanced bioremediation, e.g., [18,19], the delivery of partitioning solutes, e.g., [20], the protection and delivery of reactive particles, e.g., [13,21], enhanced contaminant recovery [22,23] and for general mobility control [24,25]. The subsurface transport of emulsions is facilitated by the physical characteristics of neutral buoyancy, modest viscosity and droplet sizes that are of the order of 1 μm [26].

Here, we report on experiments and simulations aimed at describing the rates of alkalinity release from emulsions in which alkalinity-releasing particles are located within the oil droplets of an oil-in-water emulsion. Results are compared to similar experiments and simulations designed to quantify the rates of alkalinity release from unencapsulated particles suspended within the aqueous phase.

2. Materials and Methods

2.1. Materials

Magnesium oxide and calcium carbonate particles were selected to serve as alkalinity-releasing particles, given they are commercially available in nanometer-size diameters, deemed safe for environmental use, relatively inexpensive and widely used in practice to provide alkalinity for the pH control. Magnesium oxide nanoparticles (MgO, 99% purity, $\rho = 3.58 \text{ g/mL}$) with diameters of 100 nm were obtained from Nanostructured & Amorphous Materials, Inc. (Katy, TX, USA), and reported by the manufacturer to have a specific surface area of $50 \text{ m}^2/\text{g}$. Calcium carbonate particles 60 nm in diameter (CaCO_3 , 99% purity, $\rho = 2.83 \text{ g/mL}$) were obtained from Arcos Organic (Fisher Scientific, Waltham, MA, USA). The specific surface area of the CaCO_3 particles was not reported by the manufacturer. Soybean oil (SBO, laboratory grade, $\rho = 0.920 \text{ mg/L}$ at 22°C , $\mu = 72 \text{ cP}$ at 22°C) obtained from MP Biomedicals (Irvine, CA, USA), was used as the oil phase,

given its use in environmental remediation applications. The major components of SBO are linoleate, oleate, palmitate, linolenate and stearate [27]. Gum Arabic (GA, obtained from Fisher Scientific (Waltham, MA, USA), >99% purity, $\rho = 1.36 \text{ g/mL}$) was selected as the emulsifying agent because it is a natural, nontoxic material that is frequently employed in the food industry for structural stabilization and encapsulation [28]. GA is known to contain potassium, calcium and magnesium, and may offer a limited buffering capacity [29]. Water was purified (resistivity $> 18.2 \text{ M}\Omega\cdot\text{cm}$ and total organic carbon $< 10 \text{ ppb}$) using a MilliQ gradient system (Millipore, Inc., Burlington, MA, USA).

2.2. Experiments to Support Conceptual Model Development

When encapsulating particles within oil-in-water emulsions, it is imperative that the active particles are housed within the oil phase of the emulsion to allow for a successful subsurface delivery and subsequent kinetic release. To support the conceptual understanding of particle-containing emulsions, preliminary experiments were conducted to determine how the particles behaved in the oil phase. In brief, the MgO or CaCO₃ particle–SBO dispersions were created by sonicating the mixtures for one minute (Fisher Scientific Sonic Dimembrator model 500, operated at 100% power). Particle–oil suspensions of 0.1, 0.5 and 1.0 mg-metal/g-SBO were then contacted with MilliQ water at an oil-to-aqueous ratio of 0.25 (*v/v*) in acid-washed 35 mL glass vials with Teflon-sealed caps. The vials were gently mixed (Lab Quake shaker trays) at 25 °C for 8 h, 72 h and 14 days. The sampling of the triplicate reactors was commenced by standing the vials upright for up to one hour to aid phase separation. Centrifugation was not an option, as it would have separated the particles from the oil. The lack of centrifugation resulted in a small amount of an oil–water mixture being located at the interface between the oil and aqueous phases (Figure S1). Samples were collected from each phase in the order of oil, aqueous and then interfacial mixture. The mixture was sampled for the purpose of obtaining the mass balance. Great care was taken to ensure only the desired phase was sampled. The volume of each phase was measured using 10 mL graduated (0.1 mL) conical-bottom centrifuge tubes. The metal concentration in each phase was quantified as described in Section 2.5.

2.3. Creation of Oil-in-Water Emulsions

To create the particle-containing oil-in-water emulsions, first, the particle–SBO suspension was created through sonification, as described previously. Next, an aqueous solution of 3.5% wt. GA was slowly added to a particle-in-oil suspension under well-mixed conditions (standard kitchen blender). This process created particle-containing oil-in-water emulsions via a phase inversion process.

2.4. Alkalinity Release Experiments

The alkalinity release kinetics were quantified at 22 ± 2 °C using a series of well-mixed batch experiments conducted in 500 mL reactors with approximately 350 mL of an emulsion or an aqueous suspension of nanoparticles (CaCO₃ and MgO particles). To decrease the likelihood of interactions with the atmosphere, the reactor was fitted with a cap through which the pH probe and purge gas line were passed. The headspace of the reactor was also continuously purged with nitrogen gas (N₂) to reduce the possibility of CO₂ uptake from the surroundings. Periodic additions of HCl (1 or 5 N) were used to decrease the pH and initiate periods of release for the kinetic rate experiments. The pH response was logged every five seconds using a S40 SevenMulti pH meter (Mettler Toledo). Acid additions continued until the release capacity of the emulsion or suspension was exhausted as determined by the endpoint titration to pH 4.2. The buffering capacity was also determined by titrating particle-containing emulsions with HCl to exhaustion, allowing for the calculation of the total buffering capacity based on the amount of acid added (calculation described in the Buffer Capacity Calculation Section of the Supplementary Materials). Here, we assumed that the alkalinity-releasing particles were the sole source of the buffering capacity and, thus, the percentage of the particle mass utilized could serve as a marker for the extent of

alkalinity release. It should be noted that the pH was measured and subsequently modeled in these experiments as it was a nondestructive sampling process. The continuous and dispersed phases of the emulsion could not be sampled without breaking the emulsion, which may have altered the distribution of the emulsion components. The experimental setup used for this nondestructive sampling is shown in Figure S2.

2.5. Analytical Methods

The density was measured using a 2 mL glass pycnometer (Ace Glass) calibrated with MilliQ water and verified with isopropanol prior to each day of use. The viscosity was quantified using a TA Instruments AR-G2 rheometer with a concentric cylinder geometry and reported at a shear rate of 20 s^{-1} , unless otherwise noted. The droplet size distributions were characterized using light microscopy (Ziess Axiovert S100) coupled with the MetaMorph (Molecular Devices, San Jose, CA, USA) image analysis, as well as via dynamic light scattering (Malvern Zetasizer NanoZS). The zeta potential of the emulsion droplets was assessed after dilution with MilliQ water (1:200 or 1:500) using the Malvern Zetasizer NanoZS.

Ca and Mg concentrations were quantified via inductively coupled plasma optical emission spectroscopy (ICP-OES) (7300 DV, Perkin Elmer), where the samples were introduced via a crossflow nebulizer at 0.5 mL/min. Detection was completed in the axial mode with Mg and Ca quantified at wavelengths of 279.09 and 317.93 nm, respectively, as described in the US EPA Method 6010D [30]. The instrument was calibrated using magnesium and calcium metal standard solutions (TraceCERT®Fluka Analytical, Sigma-Aldrich, St. Louis, MO, USA). The aqueous samples were acidified with concentrated nitric acid. Samples from the oil phase and interfacial mixture were dried at 105 °C until all visible water had evaporated and then heated to 550 °C for 2 h [26]. The ash remaining in each tube after heating at 550 °C was digested with 5 mL of concentrated nitric acid, placed on a shaker overnight and then diluted with MilliQ to approximately 25% nitric acid prior to the analysis.

2.6. Equilibrium Solution Chemistry

Equilibrium solution chemistry influences the rates of release through thermodynamic controls incorporated in rate expressions. The extensive chemical database “minteq.v4” that accompanies PHREEQC [31] was used for the equilibrium solution chemistry calculations of both the magnesium and calcium systems over the pH range relevant to the experiments (approximately pH 4 to pH 10). The equilibrium speciation modeling of the MgO particle emulsions was found to have an equilibrium pH value of approximately 10.5, and in the absence of other solutes, the relative amount of each magnesium species was estimated to be 91.4% Mg^{2+} , 8.08% $\text{Mg}(\text{OH})^+$, 0.48% MgCO_3 , <0.01% MgHCO_3^+ and <0.01% MgCl^- . However, at a pH of 9.5 and below, over 99% of the magnesium species were Mg^{2+} . The equilibrium pH of the CaCO_3 -containing emulsions was measured to be 8.9. At a pH value of 8.9, the soluble calcium was distributed as 97.8% Ca^{2+} , 1.9% $\text{CaCO}_3(\text{aq})$, 0.3% CaOH^+ and >0.01% CaHCO_3^+ and CaCl^+ when established in the presence of calcite and in the absence of other solutes. The activity coefficients were calculated using the extended Debye–Hückel equation. The carbonate system was included for both types of particle systems with the initial total carbonate, C_{T,CO_3} , calculated assuming that the initial water was equilibrated with the atmosphere.

The equilibrium metal ion concentration (i.e., $[\text{Ca}^{2+}]^*$ and $[\text{Mg}^{2+}]^*$) was determined by solving a system of equations that included the charge balance, carbonate speciation (Equations (1) and (2)) [32], carbonate mass balance (Equation (3)), water speciation (Equation (4)) and solubility (Equations (5)–(7)). Note that, in these equations, the curly brackets denote the activity and the square brackets denote the molar concentration.

$$\frac{\{\text{HCO}_3^-\}\{\text{H}^+\}}{\{\text{H}_2\text{CO}_3^*\}} = K_{\text{a}1} = 10^{-6.35} \quad (1)$$

$$\frac{\{CO_3^{2-}\}\{H^+\}}{\{HCO_3^-\}} = K_{a2} = 10^{-10.33} \quad (2)$$

$$C_T = [H_2CO_3^*] + [HCO_3^-] + [CO_3^{2-}] \quad (3)$$

$$\{OH^-\}\{H^+\} = K_w \quad (4)$$

$$\{Ca^{2+}\}\{CO_3^{2-}\} = K_{sp,CaCO_3} \quad (5)$$

The equilibrium Mg^{2+} concentration, Mg^{2+*} , was determined by using the solubility product equation for the solid $MgO(s)$ as follows:



$$\{Mg^{2+}\}\{OH^-\}^2 = K_{sp,MgO} \quad (7)$$

2.7. Mineral Dissolution Models

The MgO dissolution was modeled by modifying the empirical rate laws developed by Fedoročková and Raschman (2008) [33] to describe the mineral dissolution (Equation (8)). In brief, Fedoročková and Raschman (2008) [33] found the exponent in Equation (8) to be a function of temperature. The value of the exponent was determined to be 0.397 at 22 °C. Equation (8) also includes a thermodynamic control on the dissolution rate, $(1 - \Omega^2)$, with Ω defined in Equation (9) [34].

$$\frac{\partial MgO_{(s)}}{\partial t} = -k(TSA)\{H^+\}^{0.397}(1 - \Omega^2) \quad (8)$$

$$\Omega = \frac{\{Mg^{2+}\}\{OH^-\}^2}{K_{sp}} \quad (9)$$



$\frac{\partial MgO_{(s)}}{\partial t}$ represents the change in the solid particle mass per time. The curly brackets in Equations (8) and (9) denote activity. The solubility product of MgO , $K_{sp,MgO}$ in Equation (9) is defined in Equation (7), based on the dissolution reaction shown in Equation (6), and set to a value of 5.012×10^{-11} . Note that the rate law developed by Fedoročková and Raschman (2008) [33] is based upon the reaction as shown in Equation (10), and the way the reaction is written matters when considering the reported value of $K_{sp,MgO}$. That is, the $K_{sp,MgO}$ for the reaction shown in Equation (6) was the product of the $K_{sp,MgO}$ for the reaction shown in Equation (10), and the square of the water dissociation constant (i.e., K_w^2). In Equation (8), k is the rate coefficient, which was set to $7.97 \times 10^{-5} \text{ mol} \cdot \text{m}^{-2} \cdot \text{s}^{-1}$, based on the work of Fedoročková and Raschman (2008) [33]. The particles were assumed to be a uniform distribution of shrinking spheres for the purposes of calculating the total surface area (TSA) in the application of the rate expression. The MgO dissolution model was, therefore, fully parameterized using information independent from the research presented herein. All simulations conducted to describe the temporal release of alkalinity and the related pH response were performed in MATLAB R2014a (MathWorks, Natick, MA, USA). Additional information is provided in the Modeling Approach Section in the Supplementary Materials.

3. Results and Discussion

3.1. Experiments to Support Conceptual Model Development

Understanding the distribution of particle mass between the aqueous (continuous) and oil (dispersed) phases comprising an oil-in-water emulsion is difficult, given that selectively sampling one phase of an emulsion is not possible without destroying the emulsion itself. Batch experiments in this section focused on contacting particles suspended in oil with water in the absence of an emulsifier. These experiments were employed to identify the extent to which particles (i) remained suspended with an oil phase and (ii) released alkalinity to the aqueous phase. The results of these experiments guided the development of the conceptual model for the alkalinity release in subsequent experiments using particles containing oil-in-water emulsions.

The batch experiments were designed to quantify the metal content in the oil and aqueous phases as a function of contact time. As noted in the Materials and Methods Section, the centrifugation of the contacted vials was not feasible, as it would pull the particles out of the oil. Moreover, these experiments were difficult to conduct, as gravity would eventually separate the particles, the aqueous phase and the oil due to density differences (i.e., $\rho_{\text{particle}} \gg \rho_{\text{water}} > \rho_{\text{oil}}$). We used an approach that allowed for the contacted phases to gravity separate for a period of one hour. At the conclusion of this hour, some of the oil and water remained mixed near the oil–water interface. Due to our focus in these experiments being to evaluate the location of the particle mass after the contact period, we did not pursue the separation of this mixture. Rather, we quantified the mass of particles located within the interfacial region. The interfacial fraction was essentially an artifact of the mixing process employed for this test. Thus, it should not be considered representative of the interface in the emulsions stabilized with GA reported later in this paper.

The fractionation of the magnesium mass in the reactors with a mass loading of 0.1% MgO (wt. %) and contacted for 336 h (14 day) was found to be 0.81 ± 0.08 (standard deviation of triplicate reactors) in the oil, 0.06 ± 0.01 in the aqueous phase and 0.13 ± 0.02 of mass associated with the interfacial mixture (see the Fractionation Calculation Section in the Supplementary Materials for details). Additionally, the total concentrations of Mg associated with the aqueous phase ranged between 6 mg/L and 15 mg/L, with a greater mass loading and longer equilibration time producing higher concentrations (Figure 1). The aqueous solubility of Mg in these systems was estimated to be 12.7 mg/L using PHREEQC, where the particle solid was brucite (Mg(OH)_2) [31].

The total magnesium concentrations in the aqueous phase below this solubility limit suggests that the aqueous phase likely did not contain solid particles. Additionally, the slow increase in the aqueous magnesium concentrations with increasing contact time supported the hypothesis that a slow-release mechanism governs the rate. We assumed this slow step to be associated with the resistance in the mass transfer across the oil–water interface. Overall, the results demonstrate that for all particle loadings, including loadings of 1 mg/g (and likely higher), most of the total magnesium mass was present in the oil phase, even after long contact time with an aqueous phase. This proof of principle experiment was only completed for the MgO system, as the proof of concept using the CaCO_3 particles and the oil encapsulation of other particle types was previously demonstrated [13,35].

Based on the results of the experiments, the alkalinity release from the oil phase was hypothesized to follow a linear driving force model, where the release of alkalinity was limited by the exchange on the aqueous side of the oil–water interface. Support for this approach comes from Ervin et al. (2011) [36], which suggests that the diffusion within entrapped nonaqueous phase liquids (having diffusion lengths that are orders of magnitude greater than those of the emulsion droplets) may have a negligible influence on the rate of partitioning between the aqueous and organic phases. The specific linear driving force expressions used were as follows:

$$\frac{\partial [\text{Mg}^{2+}]}{\partial t} = k_{AS} ([\text{Mg}^{2+}]^* - [\text{Mg}^{2+}]) \quad (11)$$

$$\frac{\partial [\text{Ca}^{2+}]}{\partial t} = k A_s ([\text{Ca}^{2+}]^* - [\text{Ca}^{2+}]) \quad (12)$$

where $[\text{Mg}^{2+}]$ and $[\text{Ca}^{2+}]$ are the aqueous-phase concentrations of Mg^{2+} and Ca^{2+} , respectively, with dimensions of mass per volume; k is the mass transfer coefficient with dimensions of length per time; A_s specific surface area of the oil–water interface with dimensions of area per volume; $[\text{Mg}^{2+}]^*$ and $[\text{Ca}^{2+}]^*$ are the equilibrium aqueous-phase concentrations with dimensions of mass per volume.

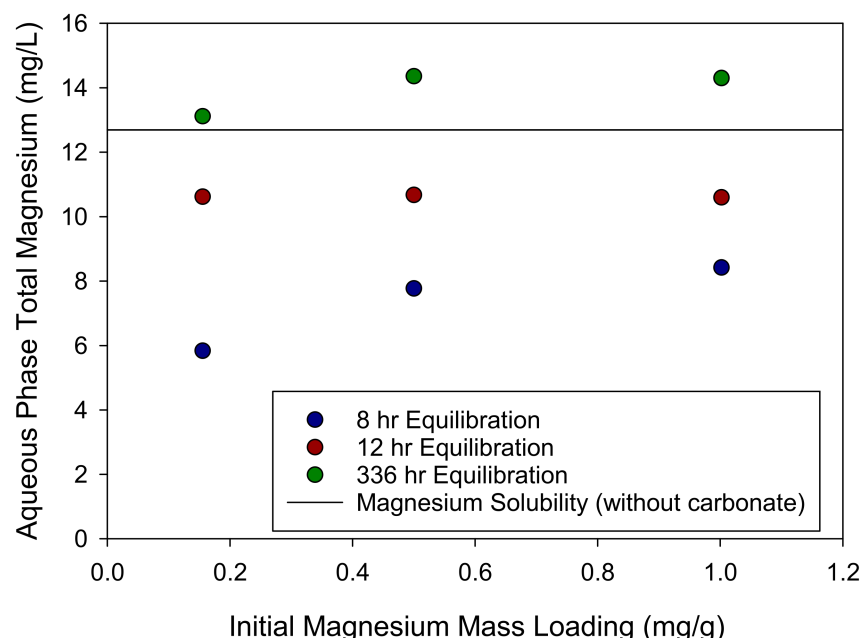


Figure 1. Measured values of total magnesium in the aqueous phase for the experiments conducted to support development of the conceptual model.

3.2. Emulsion Characterization

Emulsions containing between 0.1 and 1.0% wt. particles per wt. oil and between 20% soybean oil stabilized with 3.5% (wt.) GA and MilliQ solution were evaluated. Emulsions were characterized by the density, viscosity, droplet size and droplet zeta potential, with all characterization completed at 22.0 ± 0.2 °C. In general, all these emulsions had kinetic stabilities in excess of 20 h, densities between 0.98 and 1.01 g/mL, viscosities between 10 and 20 cP, mean droplet diameters between 1.0 and 2 µm (avg = 1.5 µm; stdev = 0.35 µm) and droplet zeta potentials between −30 and −35 mV. The exploration of the density and viscosity as a function of the oil content resulted in the use of 20% wt. SBO as the basis of the disperse phase in the oil-in-water emulsion [26]. The illustrative characterization results for the emulsions containing no particles, MgO particles, and CaCO_3 particles, respectively, are shown in Table 1. The phase inversion process used to create the emulsion promoted the particles to remain in the oil phase of the emulsion. Results from the experiments using the suspensions of particles in oil, droplet imaging and emulsion stability confirmed that the particles were held in the oil phase through the emulsification process. Together, the set of properties was consistent with those of emulsions that were demonstrated to be readily transported in sandy porous media [13,26].

Table 1. Illustrative properties of oil-in-water emulsions constructed with 20% wt. soybean oil (SBO) and stabilized with 3.5% Gum Arabic (GA).

Composition (% wt. of Emulsion)	Density (g/mL)	Viscosity (cP)	Zeta Potential (mV)	Equilibrium pH
0.02% MgO				
20% SBO			−31.43 ± 1.01	10.5
3.5% GA				
0.02% CaCO ₃				
20% SBO	0.995 ± 2.27	8.96 ± 0.14	−32.79 ± 0.90	9.8
3.5% GA				
no particles				
20% SBO			−34.82 ± 0.78	4.5
3.5% GA				

Note: ± indicates standard deviation.

3.3. Buffering Capacity

The buffering capacity of the oil-in-water emulsions encapsulating CaCO₃ and MgO particles was determined as a function of particle loading. The buffer capacity was determined from the titrations of particle-containing emulsions with the acid added normalized by the particle mass present in the emulsion. The buffer capacity was defined by an endpoint of pH 4.2 and reported in units of milliequivalents of alkalinity per gram of particles (meq-alk/g-particle). Emulsions containing MgO particles were found to have approximately 2.8 times the buffering capacity of the emulsions containing CaCO₃ particles on a per particle mass basis, as expected, based on the ratio of the stoichiometries for each alkalinity release reaction. The theoretical buffering capacities for the CaCO₃ and MgO emulsions were 20.0 and 49.6, respectively. The particle utilization—the fraction of the theoretical alkalinity that was released in the batch experiment—was found to be 72% for the encapsulated CaCO₃ particles and between 82% and 95% for the encapsulated MgO particles (Table 2).

Table 2. Buffering capacity and alkalinity utilization of emulsions containing CaCO₃ and MgO particles.

Particle Mass Loading ¹ (% wt. of Emulsion)	Measured Buffering Capacity ² (meq-alk/g-Particle)	Alkalinity Utilization (%)
0.02% CaCO ₃	14.1	70
0.03% CaCO ₃	14.4	72
0.04% MgO	40.5	82
0.03% MgO	44.7	90
0.2% MgO	45.7	92
0.4% MgO	47.1	95

Note: ¹ Oil-in-water emulsions comprising 20% particle-containing SBO stabilized with 3.5% GA. ² The buffer capacity was defined with titrating to pH 4.2.

3.4. Alkalinity Release Kinetics

The rates of alkalinity release from the emulsions encapsulating the MgO and CaCO₃ particles were determined and compared to rates determined for aqueous suspensions of the particles. The data suggest that when acid was added to the suspensions of bare particles and emulsion-encapsulated particles, the pH rebounds due to the release of alkalinity (illustrative data shown in Figures S3–S5). A comparison of the rates of alkalinity release between the bare particles and emulsion-encapsulated particles was facilitated by plotting together several of the pH recovery curves for each system (Figure 2). Note that the pH recovery curves shown in Figure 2 are for the subsequent additions of acid with the response to the first acid addition shown in grey, the second shown in red, the third shown in cyan and the fourth shown in blue. The alkalinity release and the resulting increase in

pH was slower for particles encapsulated in the emulsion droplets than it was for bare particles. Moreover, the results suggest that the particle mass loading in the emulsion systems may play a role in the release kinetics, as larger mass loading correspond with faster rates of release (Figure 3). The slower rate observed using the emulsion encapsulation approach is consistent with observations in experiments designed to aid the conceptual model development and offers a point of control. For example, the rates of release using 0.03% wt. CaCO_3 particles encapsulated within the emulsion were substantially slower than those with the same mass loading present as an aqueous suspension. This suggests that the relatively rapid rate of alkalinity release from the aqueous suspension of particles may be purposefully reduced by encapsulating the particles within the oil droplets of the emulsion. The control on the release rate afforded by the emulsion encapsulation is attributed to the additional mass transfer step imposed by the oil phase.

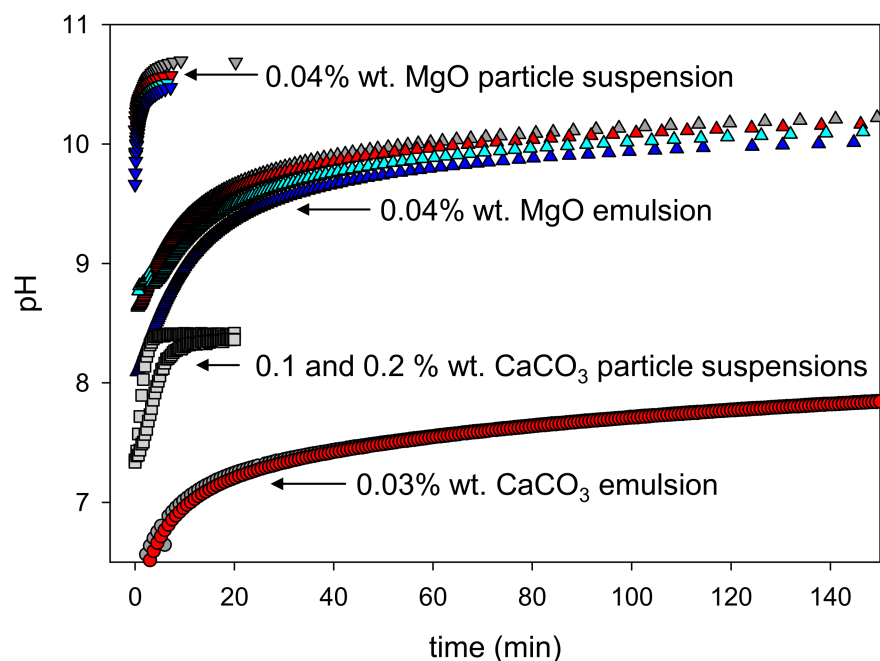


Figure 2. Measured pH during alkalinity release experiments that used repeated additions of HCl. Note that the temporal resolution of the data gives the illusion of a line, but all information shown in this figure is in the form of discrete measurements. Colors denote order of pH rebounds: first grey, second red, third cyan, fourth blue.

3.5. Modeling Rates of Release

Upon the completion of the first set of batch experiments, focus was placed on the MgO particles and, thus, most of the subsequent work relates to the MgO release behavior. MgO was selected over CaCO_3 because the MgO particles can supply nearly twice the alkalinity as the CaCO_3 particles can (per mass basis), and the utilization rate was also superior (Table 1). Thus, from a practical perspective, the MgO particles are likely to be better suited to sustain the alkalinity release over a longer term than the CaCO_3 particles, at least in terms of the amount and accessibility of the alkalinity delivered per particle mass. Additionally, magnesium is less ubiquitous than calcium in environmental systems (in both groundwater and sands), and from an experimental methods sense, using magnesium allows for better quantification of total Mg, which becomes increasingly important when assessing the transport and retention of particles in porous media.

The mineral dissolution model provides a good visual description of the MgO experiments, capturing the release kinetics from the particle suspension (illustrative data and simulation shown in Figure 4). More importantly, the model is predictive, having no adjustable parameters. The model outputs shown in Figure 5 included Mg speciation

within the aqueous phase, the value of the omega term, activity coefficients for mono-(gamma1) and divalent (gamma2) ions, ionic strength (I), average particle radius and total surface area (TSA).

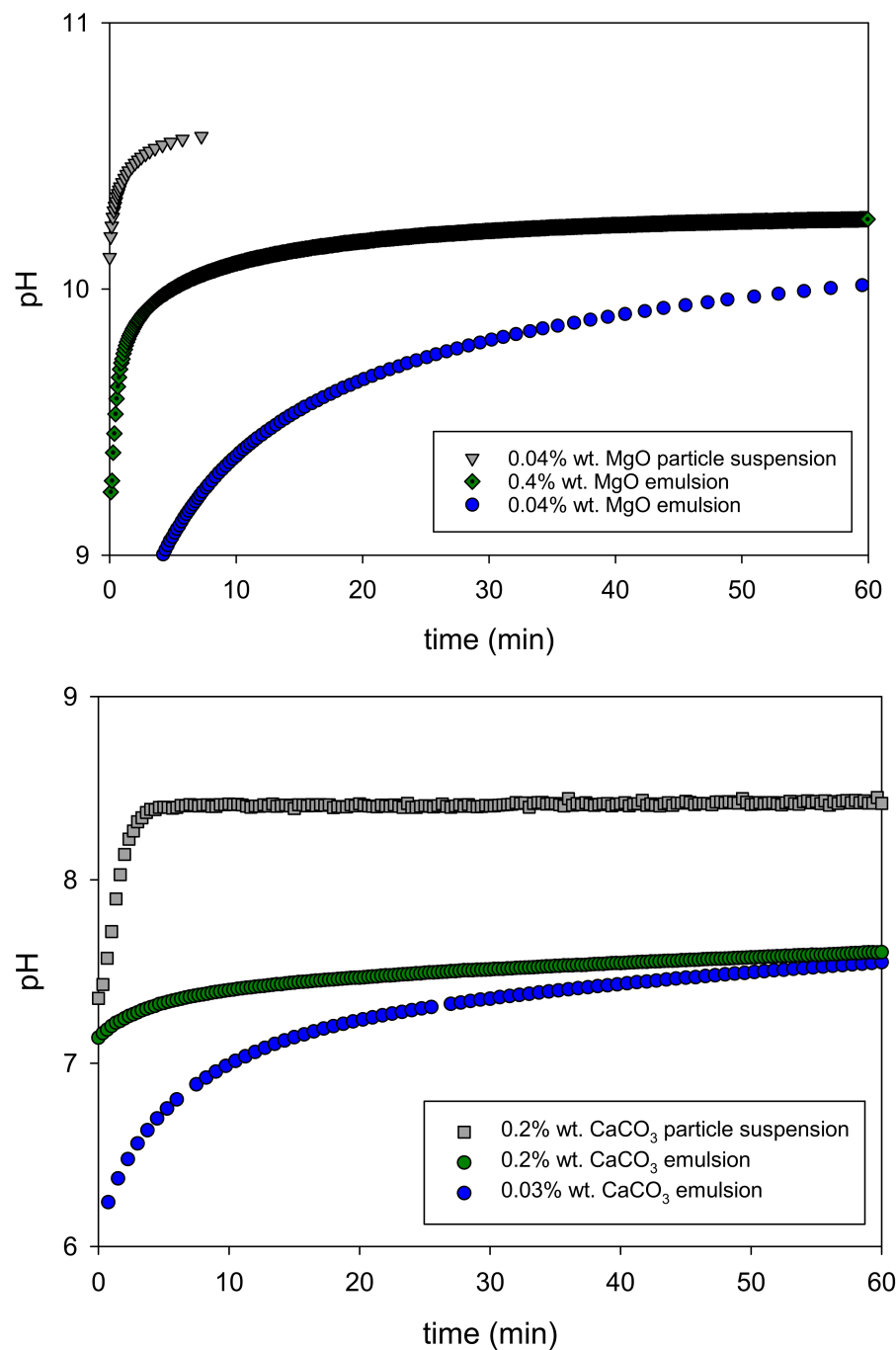


Figure 3. Illustrative pH rebound curves measured after HCl acid addition from particle suspensions and emulsions with varying mass loadings for (top) MgO and (bottom) CaCO₃. Note that the temporal resolution of the data gives the illusion of a line, but all information shown in this figure is in the form of discrete measurements.

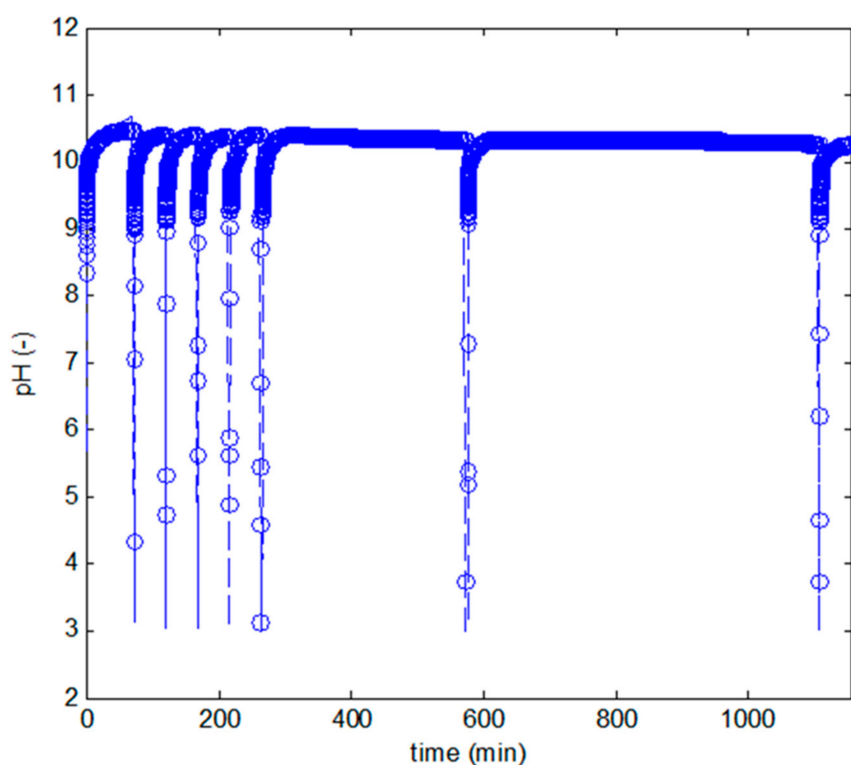


Figure 4. Measured (open circles) and simulated (line) pH responses following acid additions to a 0.04% wt. suspension of 100 nm diameter MgO nanoparticles. Simulations were produced using the mineral dissolution model described in Section 2.7.

The application of the linear driving force model to the release data measured for the particle-containing emulsions required calculating the equilibrium speciation at each time step, as the solution chemistry changes due to the alkalinity release and acid input. Additionally, the linear driving force model was refined to use a lumped mass transfer coefficient (i.e., $k_L = kA_s$), because the oil droplet size was found to remain unchanged through the alkalinity release process (Figure S6), allowing for a constant value of the lumped mass transfer coefficient throughout the release process. The linear driving force model was fit to the release data by adjusting the lumped mass transfer coefficient (k_L) and the solubility product ($K_{sp,MgO}$) (see the section on the Modeling Approach in the Supplementary Materials for additional details). Here, the value of $K_{sp,MgO}$ was allowed to vary, albeit slightly, to de-emphasize the influence of small variations in the late time equilibrium pH. This permitted the fit of k_L to better capture the kinetic release (i.e., rise toward the limit established with $K_{sp,MgO}$). The range of the adjusted $K_{sp,MgO}$ was $(1.6\text{--}2.8) \times 10^{-11}$, all of the same order of magnitude for the value used in the mineral dissolution model (5.012×10^{-11}) and with no discernable trend related to particle loading. The alkalinity release from the emulsion-encapsulated MgO particles at various loadings showed an increase in k_L with increased mass loading (Table 3). For example, k_L increased from 1.2×10^{-4} to $2.2 \times 10^{-3} \text{ min}^{-1}$ as the mass loading increased from 0.04 to 0.4% (wt./wt.). As noted previously, particle loading offers another point of control for tailoring the alkalinity release, perhaps to meet site-specific needs though the faster kinetics observed with higher mass loading. Thus, considerations of treatment duration must include the loading, utilization (Table 1) and mass transfer rate (i.e., higher loadings may have more capacity for treatment, but that capacity may be utilized faster). Our focus here was on the encapsulation and the empirical descriptions of the rates of release; however, follow-on studies may consider exploring the accessibility of the particles within the oil as a means of better understanding the dependence of k_L on particle loading.

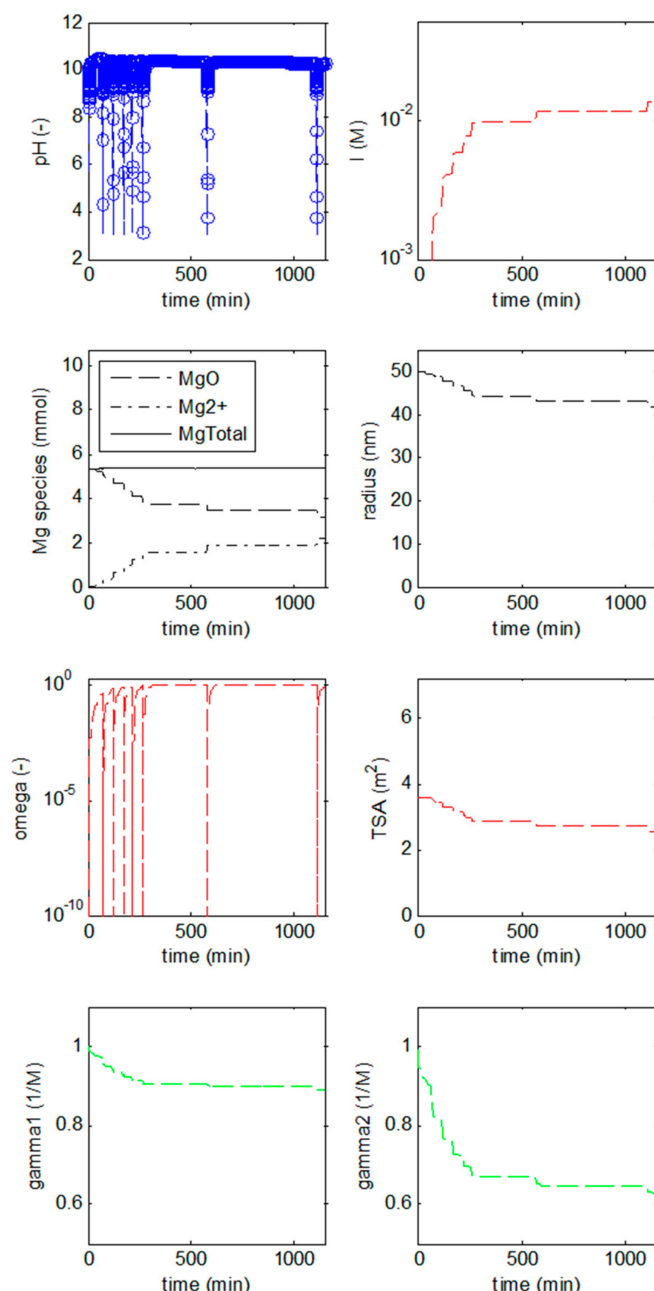


Figure 5. Time-variable properties of the mineral dissolution model: pH response as shown in Figure 4, ionic strength (I), Mg speciation, average particle radius, omega term, total particle surface area (TSA) and activity coefficients of mono- (γ_1) and divalent (γ_2) ions.

Table 3. Fitted values of the lumped mass transfer coefficient (k_L) and solubility product ($K_{sp,MgO}$) for the linear driving force model used to describe the alkalinity release kinetics from MgO particle-containing oil-in-water emulsions.

Emulsion Particle Content ¹ (% wt. of Emulsion)	k_L (min ⁻¹)	$K_{sp,MgO}$
0.04% MgO	1.2×10^{-4}	2.8×10^{-11}
0.1% MgO	2.6×10^{-4}	2.0×10^{-11}
0.2% MgO	1.8×10^{-3}	1.6×10^{-11}
0.4% MgO	1.0×10^{-3}	2.8×10^{-11}

Note: ¹ Oil-in-water emulsions comprising 20% particle-containing SBO stabilized with 3.5% GA.

To explore whether some of the particles at loadings of 0.2 and 0.4% mass per mass may have been present within the aqueous phase (i.e., not encapsulated within the dispersed oil phase), the mineral dissolution and linear driving force models were combined on a fractional contribution basis, that is one kinetic contribution from the aqueous-phase particles via the mineral dissolution model and another kinetic contribution from the encapsulated particles via the linear driving force model. The aim here was to test the hypothesis that the combined model could describe the pH data and, thus, offer a reasonable description of the alkalinity release kinetics. We tested the hypothesis by varying the fraction of particles not encapsulated (i.e., those having a fast response via the mineral dissolution model, f_{fast}) and fitting the lumped mass transfer coefficient associated with the encapsulated fraction ($1 - f_{\text{fast}}$). The results suggest that mineral dissolution mechanisms are not able to describe the alkalinity release from these emulsions (Figure 6 shows illustrative results). The best fitting results were obtained when the fraction of bare particles was zero (i.e., $f_{\text{fast}} = 0$), indicative of all particles being encapsulated within the oil droplets of the emulsion. Additional evidence for encapsulation came from the 0.4% MgO emulsion modeling results (at early time), where $f_{\text{fast}} = 2 \times 10^{-7}$ and $k_L = 1.7 \times 10^{-5} \text{ min}^{-1}$. Shown in Figure 6 are illustrative results for the sensitivity of the modeled release rate to the possible fraction of particles in the aqueous phase. Notice that the release kinetics visually overshot the observed data when 5% or more of the particles were assumed to be unencapsulated. The results from the release modeling reinforced the earlier finding that particles in the oil were associated with the oil phase (Figure 1).

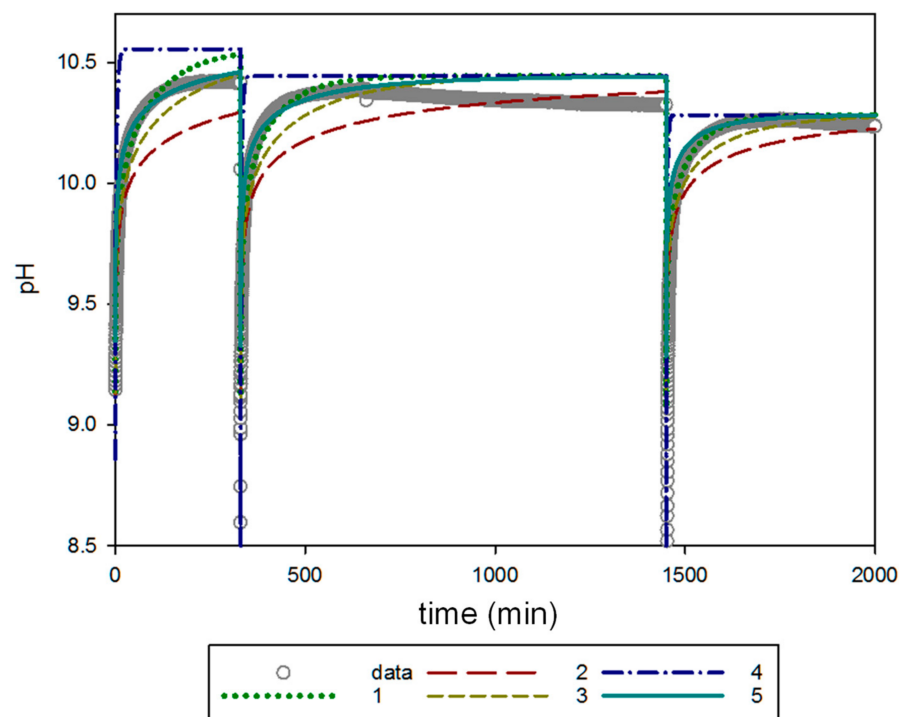


Figure 6. Simulations conducted to explore the possible influence of particles not encapsulated within the oil droplets of an emulsion containing 0.1% wt. MgO. Measured pH is shown as the grey open circles. Note that the temporal resolution of discrete pH measurements gave the illusion of a line. The lumped mass transfer coefficient, k_L , was fit to a series of hypothetical fractions of unencapsulated particles, f_{fast} . Simulations: (1—dashed line) $f_{\text{fast}} = 0.05$ produced a best fit k_L of $6.1 \times 10^{-5} \text{ min}^{-1}$; (2—medium dashed line) $f_{\text{fast}} = 0.00025$ produced a best fit k_L of $6.0 \times 10^{-5} \text{ min}^{-1}$; (3—short dashed line) $f_{\text{fast}} = 0.025$ produced a best fit k_L of $6.0 \times 10^{-5} \text{ min}^{-1}$; (4—dot and dashed line) $f_{\text{fast}} = 0.99$ produced a best fit k_L of $6.0 \times 10^{-6} \text{ min}^{-1}$; and (5—solid line) $f_{\text{fast}} = 0$ produced a best fit k_L of $2.7 \times 10^{-4} \text{ min}^{-1}$ and. All models were run with $k_{\text{diss}} = 1.2 \times 10^{-3} \text{ min}^{-1}$ and $K_{\text{sp,MgO}} = 5.01 \times 10^{-11}$.

4. Implications

The research described herein built upon our prior work in encapsulating reactive iron particles in oil and water emulsions, e.g., [13,28] to examine the encapsulation of MgO and CaCO₃ alkalinity-releasing nanoparticles. The experimental results indicate that a large fraction of the particles was encapsulated at all particle loadings. Even at mass loadings of 1 mg·g⁻¹ (and likely higher), most of the total magnesium mass was present in the oil even after an extended contact time with an aqueous phase. The emulsification of the particle-containing oil was found to encapsulate the particles and slow the rate of the alkalinity release. Moreover, 80–90% of the encapsulated MgO particle mass remained accessible for release into the aqueous phase.

We found that a linear driving force model well described the slower release of alkalinity observed for the encapsulated particles when compared with rates of mineral dissolution of bare particles. The hypothesis that a slow-release mechanism governed the release rate was supported by the observation of a slow increase in aqueous-phase magnesium concentrations when water was in contact with an oil phase that contained particles. The attenuation of the alkalinity release (from the rate of mineral dissolution that would be expected with bare particles) was attributed to a resistance in the mass transfer across the oil–water interface. This has important implications for controlling the rate of the release of alkalinity. Bare particles suspended within the aqueous phase released alkalinity with rates that were linear in pH (Figure 7). In contrast, the alkalinity release from encapsulated particles was expected to be largely independent of pH, except at those values of pH that were within a unit of the equilibrium, aqueous-phase concentration. In contrast to millimeter-scale encapsulation methods, e.g., [37], emulsions such as those used in this study have been shown to be readily transported within porous media, which is critical for amendment delivery, e.g., [13,26].

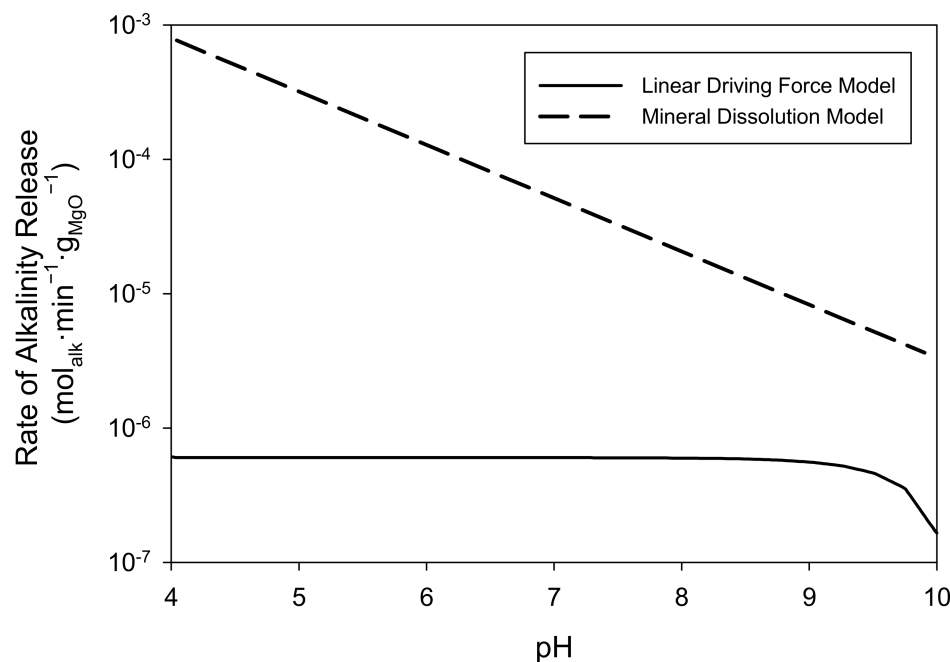


Figure 7. Comparison of the mineral dissolution model used to describe rates of alkalinity release from aqueous suspensions of particles and the linear driving force model used to describe rates of alkalinity release from particles encapsulated in the oil droplets of an oil-in-water emulsion. Note that the release rates are shown on a log scale.

Supplementary Materials: The following supporting information can be downloaded at: <https://www.mdpi.com/article/10.3390/w15081611/s1>, Figure S1: phases present in the experiments described in Section 3.1; Figure S2: experimental setup for nondestructive sampling of emulsions

and particle suspensions described in Sections 3.3 and 3.4; Figure S3: alkalinity release in response to repeated additions of HCl into an aqueous suspension of 0.04% wt. MgO particles; Figure S4: alkalinity release from an oil-in-water emulsion containing 0.04% wt. MgO particles; Figure S5: alkalinity release from an oil-in-water emulsion containing 0.02% wt. CaCO₃ particles; Figure S6: illustrative data showing emulsion droplet sizes through the alkalinity release process; Figure S7: equilibrium chemistry via PHREEQC; Figure S8: overall modeling approach; Table S1: notes for Figures S7 and S8; as well as information on the fractionation calculation, buffer capacity calculation and modeling approach.

Author Contributions: K.A.M.: Investigation, Methodology, Visualization and Writing—Original Draft; C.A.R.: Conceptualization, Funding Acquisition, Project Administration, Supervision and Writing—review and editing. All authors have read and agreed to the published version of the manuscript.

Funding: This research was supported by the United States National Science Foundation through grant CMMI-1000714. Any opinions, findings, conclusions or recommendations expressed in this material are those of the authors and do not necessarily reflect the views of the sponsor.

Institutional Review Board Statement: Not applicable.

Informed Consent Statement: Not applicable.

Data Availability Statement: The data presented in this study are available from the corresponding author upon request.

Acknowledgments: The authors gratefully acknowledge the contributions of the anonymous reviewers in strengthening the manuscript. The authors express appreciation to Chris Martin for his assistance with some of the measurements.

Conflicts of Interest: The authors declare no conflict of interest.

References

1. Vainberg, S.; Condee, C.W.; Steffan, R.J. Large-scale production of bacterial consortia for remediation of chlorinated solvent-contaminated groundwater. *J. Ind. Microbiol. Biotechnol.* **2009**, *36*, 1189–1197. [[CrossRef](#)] [[PubMed](#)]
2. Lacroix, E.; Brovelli, A.; Barry, D.A.; Holliger, C. Use of Silicate Minerals for pH Control during Reductive Dechlorination of Chloroethenes in Batch Cultures of Different Microbial Consortia. *Appl. Environ. Microbiol.* **2014**, *80*, 3858–3867. [[CrossRef](#)] [[PubMed](#)]
3. Ortiz-Medina, J.F.; Yuncu, B.; Ross, L.; Elkins, B. The importance of proper pH adjustment and control to achieve complete in situ enhanced reductive dechlorination. *Integr. Environ. Assess. Manag.* **2022**. [[CrossRef](#)]
4. McCarty, P.L.; Chu, M.-Y.; Kitanidis, P.K. Electron donor and pH relationships for biologically enhanced dissolution of chlorinated solvent DNAPL in groundwater. *Eur. J. Soil Biol.* **2007**, *43*, 276–282. [[CrossRef](#)]
5. Amos, B.K.; Suchomel, E.J.; Pennell, K.D.; Löfller, F.E. Microbial activity and distribution during enhanced contaminant dissolution from a NAPL source zone. *Water Res.* **2008**, *42*, 2963–2974. [[CrossRef](#)]
6. Robinson, C.; Barry, D.; McCarty, P.L.; Gerhard, J.I.; Kouznetsova, I. pH control for enhanced reductive bioremediation of chlorinated solvent source zones. *Sci. Total Environ.* **2009**, *407*, 4560–4573. [[CrossRef](#)] [[PubMed](#)]
7. Hiortdahl, K.M.; Borden, R.C. Enhanced Reductive Dechlorination of Tetrachloroethene Dense Nonaqueous Phase Liquid with EVO and Mg(OH)₂. *Environ. Sci. Technol.* **2013**, *48*, 624–631. [[CrossRef](#)]
8. Muller, K.A.; Johnson, C.D.; Bagwell, C.E.; Truex, M.J. Methods for Delivery and Distribution of Amendments for Subsurface Remediation: A Critical Review. *Groundw. Monit. Remediati.* **2020**, *41*, 46–75. [[CrossRef](#)]
9. Piegat, J.; Newman, W.A. Maintaining neutral pH in deep soils and ground water utilizing insoluble colloidal buffers. In Proceedings of the Sixth International Conference on Remediation of Chlorinated and Recalcitrant Compounds, Monterey, CA, USA, 19–22 May 2008; Paper E-023. Battelle: Columbus, OH, USA. ISBN 1-57477-163-9. Available online: www.battelle.org/chlorcon (accessed on 17 April 2023).
10. Zhong, L.; Truex, M.; Kananizadeh, N.; Li, Y.; Lea, A.; Yan, X. Delivery of vegetable oil suspensions in a shear thinning fluid for enhanced bioremediation. *J. Contam. Hydrol.* **2015**, *175–176*, 17–25. [[CrossRef](#)]
11. Oostrom, M.; Truex, M.J.; Vermeul, V.R.; Zhong, L.; Tartakovsky, G.D.; Wietsma, T.W. Remedial Amendment Delivery Near the Water Table Using Shear Thinning Fluids: Experiments and Numerical Simulations. *Environ. Process.* **2014**, *1*, 331–351. [[CrossRef](#)]
12. Abriola, L.M.; Drummond, C.D.; Hahn, E.J.; Hayes, K.F.; Kibbey, T.C.G.; Lemke, L.D.; Pennell, K.D.; Petrovskis, E.A.; Ramsburg, C.A.; Rathfelder, K.M. Pilot-Scale Demonstration of Surfactant-Enhanced PCE Solubilization at the Bachman Road Site. Site Characterization and Test Design. *Environ. Sci. Technol.* **2005**, *39*, 1778–1790. [[CrossRef](#)]
13. Berge, N.D.; Ramsburg, C.A. Oil-in-Water Emulsions for Encapsulated Delivery of Reactive Iron Particles. *Environ. Sci. Technol.* **2009**, *43*, 5060–5066. [[CrossRef](#)] [[PubMed](#)]

14. Rust, C.M.; Aelion, C.; Flora, J.R. Laboratory sand column study of encapsulated buffer release for potential in situ pH control. *J. Contam. Hydrol.* **2001**, *54*, 81–98. [[CrossRef](#)] [[PubMed](#)]
15. Liu, L.; Baker, B.; Flora, J.R.V.; Aelion, C.M. Kinetics of Acidic Macrocapsules in Controlling the pH of Groundwater. *Environ. Eng. Sci.* **2008**, *25*, 1345–1356. [[CrossRef](#)]
16. Aelion, C.M.; Davis, H.T.; Flora, J.R.; Kirtland, B.C.; Amidon, M.B. Application of encapsulation (pH-sensitive polymer and phosphate buffer macrocapsules): A novel approach to remediation of acidic ground water. *Environ. Pollut.* **2009**, *157*, 186–193. [[CrossRef](#)]
17. Borden, R.C.; Richardson, S.D.; Bodour, A.A. Enhanced reductive dechlorination of trichloroethene in an acidic DNAPL impacted aquifer. *J. Environ. Manag.* **2019**, *237*, 617–628. [[CrossRef](#)]
18. Borden, R.C.; Lee, M.D. Method for Remediation of Aquifers. U.S. Patent RE40734 E1, 16 June 2009.
19. Watson, D.B.; Wu, W.-M.; Mehlhorn, T.; Tang, G.; Earles, J.; Lowe, K.; Gihring, T.M.; Zhang, G.; Phillips, J.; Boyanov, M.I.; et al. In Situ Bioremediation of Uranium with Emulsified Vegetable Oil as the Electron Donor. *Environ. Sci. Technol.* **2013**, *47*, 6440–6448. [[CrossRef](#)] [[PubMed](#)]
20. Ramsburg, C.A.; Pennell, K.D.; Kibbey, T.C.G.; Hayes, K.F. Use of a Surfactant-Stabilized Emulsion to Deliver 1-Butanol for Density-Modified Displacement of Trichloroethene. *Environ. Sci. Technol.* **2003**, *37*, 4246–4253. [[CrossRef](#)]
21. Quinn, J.; Geiger, C.; Clausen, C.; Brooks, K.; Coon, C.; O’Hara, S.; Krug, T.; Major, D.; Yoon, W.-S.; Gavaskar, A.; et al. Field Demonstration of DNAPL Dehalogenation Using Emulsified Zero-Valent Iron. *Environ. Sci. Technol.* **2005**, *39*, 1309–1318. [[CrossRef](#)]
22. Lee, Y.-C.; Kwon, T.-S.; Yang, J.-S.; Yang, J.-W. Remediation of groundwater contaminated with DNAPLs by biodegradable oil emulsion. *J. Hazard. Mater.* **2007**, *140*, 340–345. [[CrossRef](#)]
23. Ramsburg, C.A.; Baniahmad, P.; Muller, K.A.; Robinson, A.D. Emulsion-based recovery of a multicomponent petroleum hydrocarbon NAPL using nonionic surfactant formulations. *J. Contam. Hydrol.* **2023**, *255*, 104144. [[CrossRef](#)] [[PubMed](#)]
24. Zhong, L.; Oostrom, M.; Wietsma, T.; Covert, M. Enhanced remedial amendment delivery through fluid viscosity modifications: Experiments and numerical simulations. *J. Contam. Hydrol.* **2008**, *101*, 29–41. [[CrossRef](#)] [[PubMed](#)]
25. Guillen, V.R.; Romero, M.I.; Carvalho, M.D.S.; Alvarado, V. Capillary-driven mobility control in macro emulsion flow in porous media. *Int. J. Multiph. Flow* **2012**, *43*, 62–65. [[CrossRef](#)]
26. Muller, K.A.; Esfahani, S.G.; Chapra, S.C.; Ramsburg, C.A. Transport and Retention of Concentrated Oil-in-Water Emulsions in Porous Media. *Environ. Sci. Technol.* **2018**, *52*, 4256–4264. [[CrossRef](#)]
27. Hammond, E.G.; Johnson, L.A.; Su, C.; Wang, T.; White, P.J. Soybean Oil. In *Bailey’s Industrial Oil and Fat Products*; John Wiley & Sons: Hoboken, NJ, USA, 2005. [[CrossRef](#)]
28. Long, T.; Ramsburg, C.A. Encapsulation of nZVI particles using a Gum Arabic stabilized oil-in-water emulsion. *J. Hazard. Mater.* **2011**, *189*, 801–808. [[CrossRef](#)]
29. NPCS Board of Consultants & Engineers. Chapter 19 Gum Arabic. In *Handbook on Textile Auxiliaries, Dyes and Dye Intermediates Technology*; Asia Pacific Business Press Inc.: Delhi, India, 2009; pp. 353–375.
30. United States Environmental Protection Agency. *Method 6010D: Inductively Coupled Plasma-Optical Emission Spectrometry (ICP-OES), Test Methods for Evaluating Solid Waste, Physical/Chemical Methods*, EPA publication SW-846; US EPA: Washington, DC, USA, 2014.
31. Parkhurst, D.L.; Appelo, C.A.J. Description of input and examples for PHREEQC version 3—A computer program for speciation, batch-reaction, one-dimensional transport, and inverse geochemical calculations. *US Geol. Surv. Tech. Methods* **2013**, *6*, 497.
32. Benjamin, M.M. *Water Chemistry*; Waveland Press: Long Grove, IL, USA, 2014.
33. Fedoročková, A.; Raschman, P. Effects of pH and acid anions on the dissolution kinetics of MgO. *Chem. Eng. J.* **2008**, *143*, 265–272. [[CrossRef](#)]
34. Pokrovsky, O.S.; Schott, J. Experimental study of brucite dissolution and precipitation in aqueous solutions: Surface speciation and chemical affinity control. *Geochim. Cosmochim. Acta* **2004**, *68*, 31–45. [[CrossRef](#)]
35. Ramsburg, C.A.; Almquist, J.K.; Leach, O.I. Exploration of the Mechanisms Controlling Emulsion-Based Alkalinity Release during Subsurface Remediation. In Proceedings of the 2011 NSF Engineering Research and Innovation Conference, Atlanta, GA, USA, 4–7 January 2011.
36. Ervin, R.E.; Boroumand, A.; Abriola, L.M.; Ramsburg, C.A. Kinetic limitations on tracer partitioning in ganglia dominated source zones. *J. Contam. Hydrol.* **2011**, *126*, 195–207. [[CrossRef](#)]
37. Rust, C.M.; Aelion, C.; Flora, J.R. Control of pH during denitrification in subsurface sediment microcosms using encapsulated phosphate buffer. *Water Res.* **2000**, *34*, 1447–1454. [[CrossRef](#)]

Disclaimer/Publisher’s Note: The statements, opinions and data contained in all publications are solely those of the individual author(s) and contributor(s) and not of MDPI and/or the editor(s). MDPI and/or the editor(s) disclaim responsibility for any injury to people or property resulting from any ideas, methods, instructions or products referred to in the content.